Electronic Supplementary Information (ESI) for:

Microplasma-Chemical Synthesis and Tunable Real-time Plasmonic Responses of Alloyed Au_xAg_{1-x} Nanoparticles

Tingting Yan,[a] Xiao Xia Zhong,[*a] Amanda Evelyn Rider,[b,c] Yi Lu,[a] Scott A. Furman,[b] and Kostya (Ken) Ostrikov[*b,c,d]

[a] Shanghai Jiao Tong University, Shanghai 200240, P. R. China.

[b] CSIRO Materials Science & Engineering, Lindfield, NSW 2070, Australia

[c] Faculty of Science, The University of Sydney, NSW 2006, Australia

[d] University of Technology Sydney, PO Box 123, Broadway NSW 2007, Australia

*E-mails: xxzhong@sjtu.edu.cn; kostya.ostrikov@csiro.au

Contents:

S1: Experimental Details

Plasma reduction of a $HAuCl_4$ and $AgNO_3$ mixed solution was used to synthesize Au-Ag alloy NPs (as described in Figure 1(b-c)). A Pt foil electrode (DJS-1, φ12×120, INESA Scientific Instrument Co. Ltd), which served as an anode, was immersed in the electrolyte and was positioned 2-3 cm away from the cathode which was a stainless-steel capillary (175 μm inside diameter, 10 cm length, Unimicro Technologies Inc.) with the opening 1-2 mm above the electrolyte surface.

The electrolyte was composed of silver nitrate, chloroauric acid and fructose (a stabilizer that prevents uncontrolled particle growth and agglomeration, this is discussed in more detail in S8 of the SI). The concentration of $HAuCl_4$ and $AgNO_3$ was adjusted to 5.0×10^{-5} M (with the ratio of Au and Ag being 1:4 - the amount of $HAuCl_4$ being limited to avoid an overabundance of Cl^-), to avoid the precipitation of AgCl. The concentration of fructose was 5.0×10^{-2} M.

By coupling the capillary tube with 25 sccm helium gas and applying a high dc voltage (~1 kV) to the anode, the microplasma was generated in the gas phase over the surface of electrolyte. The volume of the electrolyte is 5 mL, the discharge current was kept constant at 5 mA during the reduction. The solutions were analyzed *in situ* by using AvaLight-DH-S-BAL as the light source of the absorbance spectra and the Avaspec-2048-2-USB2 as the detector of the UV-Vis absorbance spectra (peak fitting of absorbance spectra described in Section S5). The morphology of Au_xAg_{1-x} NPs was studied by using transmission electron microscope (TEM) at an accelerating voltage of 200 kV (TEM, JEM-2100F).

S2: Estimate of energy required for microplasma-method vs citrate method

Microplasma-based method

A voltage of ~1 kV is needed to ignite the plasma, which takes approximately 1 seconds (note, it can actually be a little less). The discharge current is 5mA.

Power = 1 kV · 5 mA = 5 J/s

Energy expended for ignition: E = 5 [J/s] * 1 [s] = 5 J

Once the plasma has ignited, the voltage decreases from 900 V to 500 V. For the sake of this estimate, we will take the average value of 700 V

Hence, Total energy required = Energy required for ignition + energy required during the microplasma exposure

1. Total energy expended for 1 min: 5 J + [60*(0.7 kV*5mA)] = 5 J + 210 J = 215 J
2. Total energy expended for 2 min: 5 J + [120*(0.7 kV*5mA)] = 5 J + 420 J = 425 J
3. Total energy expended for 3 min: 5 J + [180*(0.7 kV*5mA)] = 5 J + 630 J = 635 J
4. Total energy expended for 4 min: 5 J + [240*(0.7 kV*5mA)] = 5 J + 840 J = 845 J

Citrate-based method:

This involves heating ~95 mL of solution to boiling. Let us assume we start at room temperature 25 ^{o}C and raise the temperature to 100 ^{o}C (hence ΔT = 75 K), we'll be using the basic data of H_2O for this example.

$Q = mc\Delta T = 0.095 \cdot 4190 \cdot 75 = 2.99 \times 10^4$ J

where Q is the heat required to raise 95 mL of water from 25 ^{o}C to 100 ^{o}C and c is the specific heat capacity of H_2O. This estimate does not even consider how much energy it takes to keep it boiling for another 35 min as required by standard processes.

Assume a bath with a power output of 1.3 kW, if ran for 35 min → $E_{output} = 2.73 \times 10^6$ J.

Therefore, the minimum energy cost is $(2.73 \times 10^6) + (2.99 \times 10^4)$ J → 2.76×10^6 J

We can thus conclude that our plasma-based method is more energy efficient by at least a factor of 10, most likely considerably more (i.e. factor of 1000, if one considers the energy required to maintain the temperature during the very long commonly used synthesis process).

Comment: We note that our choice of reactions for comparison was prompted by the ubiquity of the citrate technique. We stress that the most important factor in this comparison is proof of principle, i.e. whether the alloyed, crystalline AuAg nanoparticles can be synthesized or not. Our technique is not yet at mass production stage, and this point is clearly outside the scope of this work. However, we acknowledge the need for the future study of the scalability of this method and the associated increase in the mass production of the nanoparticles. The production yield estimates will be carried out during the optimization and scale up stage.

S3: More Au_xAg_{1-x} overview TEMs and particle size distributions

This section contains a range of TEMs for Au_xAg_{1-x} NPs synthesized with 1 to 4 min microplasma exposure. Particle size distributions (PSD) based on TEM measurements (bin sizes were 0.2 nm, PSD data was plotted against the median value of the range - i.e. if 5 - 5.2, then it was plotted against 5.1) as well as associated Gaussian fit (see Equation S3.1, below) data is provided.

$$y = y_0 + \frac{A}{w\sqrt{\pi/2}} e^{-2\frac{(x-x_c)^2}{w^2}}, \qquad \text{(S3.1)}$$

Further details of these distributions are included in the figure captions.

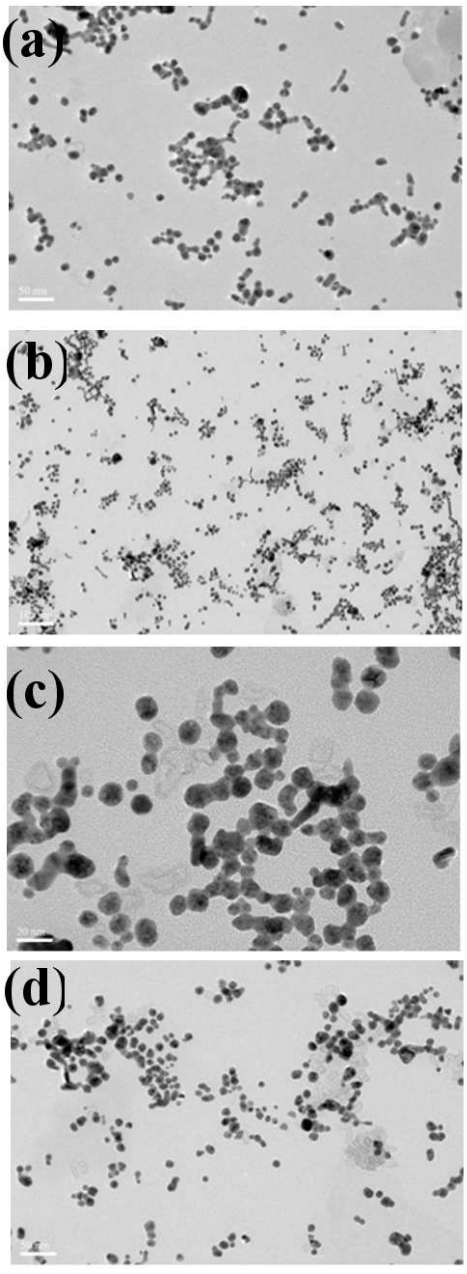

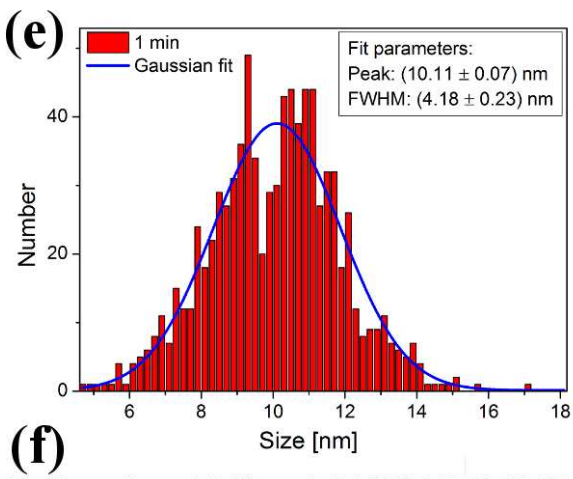

(f)

Nonlinear Curve Fit (Gauss) (23/05/2013 10:03:59)

Parameters

		Value	Standard Error
Number	y0	0.13132	0.98313
	xc	10.10719	0.07414
	w	3.55061	0.19357
	A	173.18001	11.14169
	sigma	1.7753	0.09678
	FWHM	4.18052	0.22791
	Height	38.9166	1.57559

Reduced Chi-sqr = 20.7775932054
COD(R^2) = 0.90604040264066
Iterations Performed = 6
Total Iterations in Session = 7
Fit converged. Chi-Sqr tolerance value of 1E-9 was reached.
sigma, FWHM, Height are derived parameter(s).

Statistics

	Number
Number of Points	68
Degrees of Freedom	64
Reduced Chi-Sqr	20.77759
Residual Sum of Squares	1329.76597
Adj. R-Square	0.90164
Fit Status	Succeeded(100)

Fit Status Code :
100 : Fit converged. Chi-Sqr tolerance value of 1E-9 was reached

Figure S3-1: More TEMs for samples synthesized at 1 min microplasma exposure (scale bars: (a) 50 nm, (b) 100 nm, (c) 20 nm, (d) 50 nm) and (e) PSD with fitted gaussian, (f) Origin fit report – parameters as in S3.1 (e&f) based on 874 measurements sorted into 0.2 nm bins from 4.6 nm to 18.2 nm. Note one measurement of 0.16 nm appeared to be an outlier and was excluded from fit analysis, the next smallest value was 4.7 nm. From the raw data, min. size = 4.7 nm, max. size = 17.05 nm.

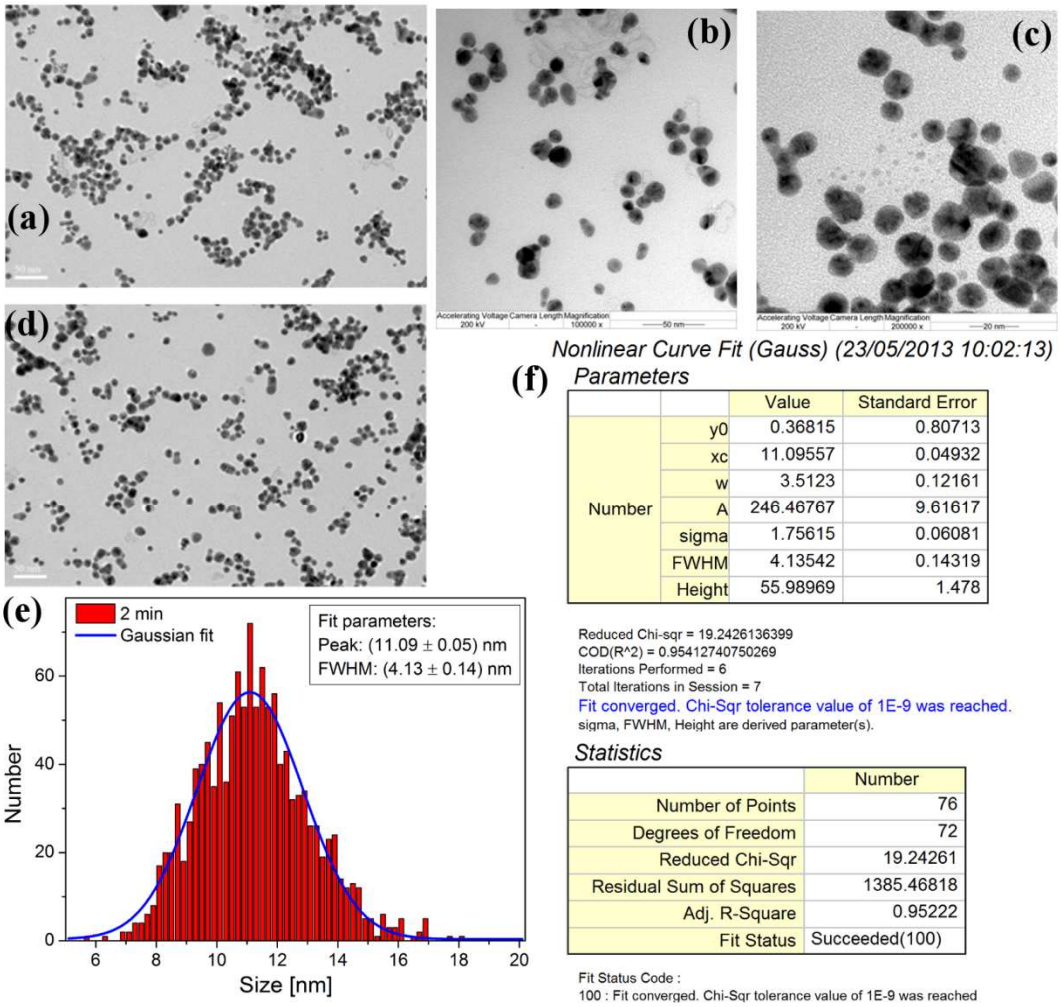

Nonlinear Curve Fit (Gauss) (23/05/2013 10:02:13)

(f) *Parameters*

		Value	Standard Error
Number	y0	0.36815	0.80713
	xc	11.09557	0.04932
	w	3.5123	0.12161
	A	246.46767	9.61617
	sigma	1.75615	0.06081
	FWHM	4.13542	0.14319
	Height	55.98969	1.478

Reduced Chi-sqr = 19.2426136399
COD(R^2) = 0.95412740750269
Iterations Performed = 6
Total Iterations in Session = 7
Fit converged. Chi-Sqr tolerance value of 1E-9 was reached.
sigma, FWHM, Height are derived parameter(s).

Statistics

	Number
Number of Points	76
Degrees of Freedom	72
Reduced Chi-Sqr	19.24261
Residual Sum of Squares	1385.46818
Adj. R-Square	0.95222
Fit Status	Succeeded(100)

Fit Status Code :
100 : Fit converged. Chi-Sqr tolerance value of 1E-9 was reached

Figure S3-2: More TEMs for samples synthesized at 2 min microplasma exposure (scale bars: (a) 50 nm, (b) 20 nm, (c) 20 nm, (c) 50 nm) and a (e) PSD with a fitted gaussian, (f) Origin fit report – parameters as in S3.1. (e & f) based on 1260 measurements sorted into 0.2 nm bins from 5 nm to 20.2 nm). From the raw data, min. size = 5.7 nm, max. size = 18.16 nm

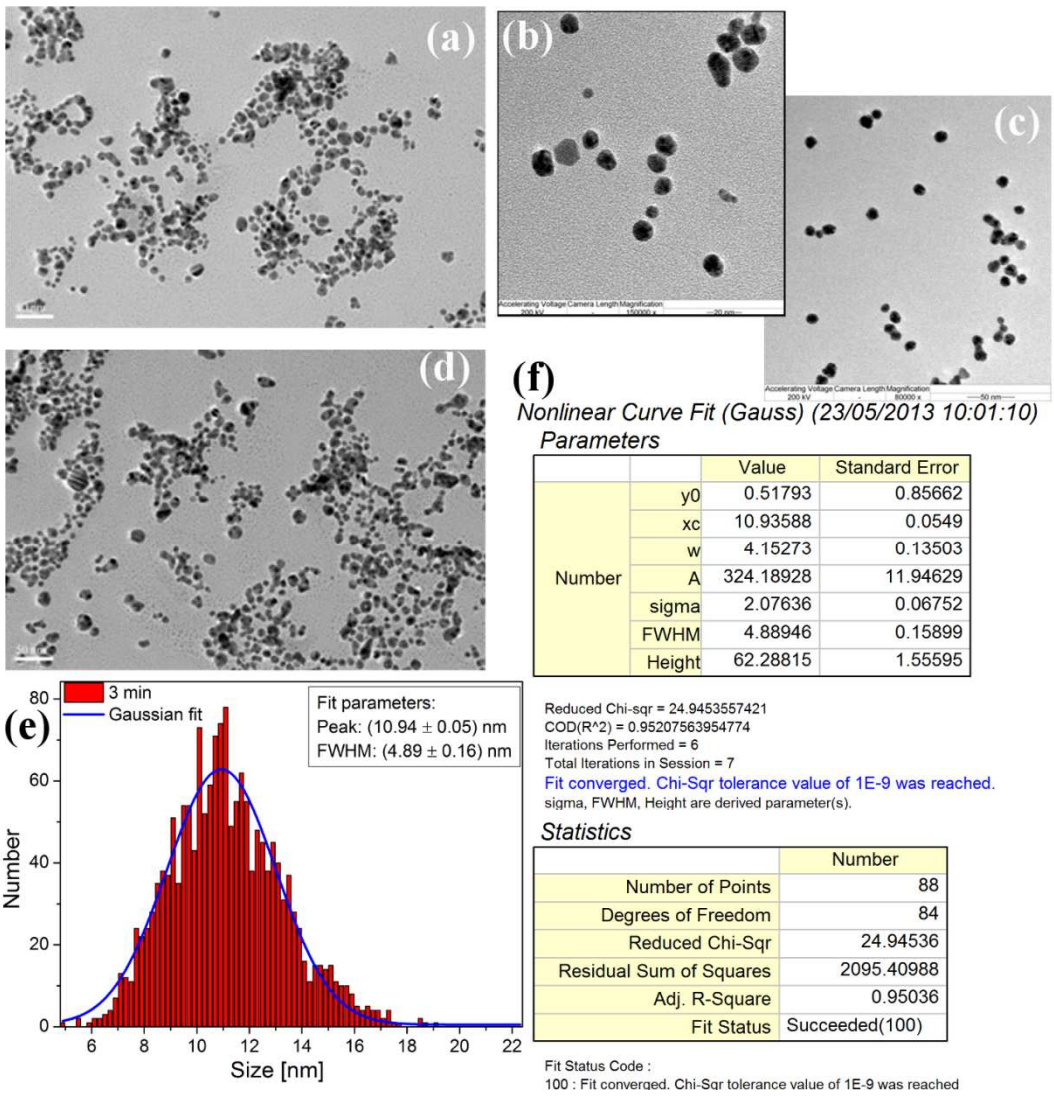

Figure S3-3: More TEMs for samples synthesized at 3 min microplasma exposure (scale bars: (a) 50 nm, (b) 20 nm, (c) 20 nm, (d) 50 nm) and a (e) PSD with a fitted gaussian, (f) Origin fit report – parameters as in S3.1. (e&f) based on 1664 measurements sorted into 0.2 nm bins from 4.8 nm to 22.4 nm. From the raw data, min. size = 4.87 nm, max. size = 19.01 nm

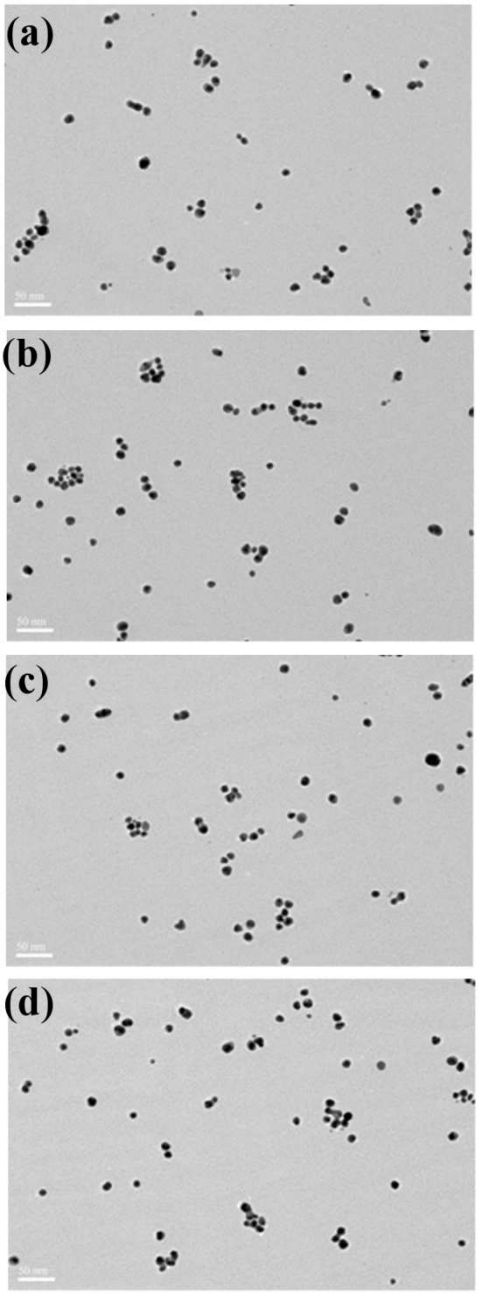

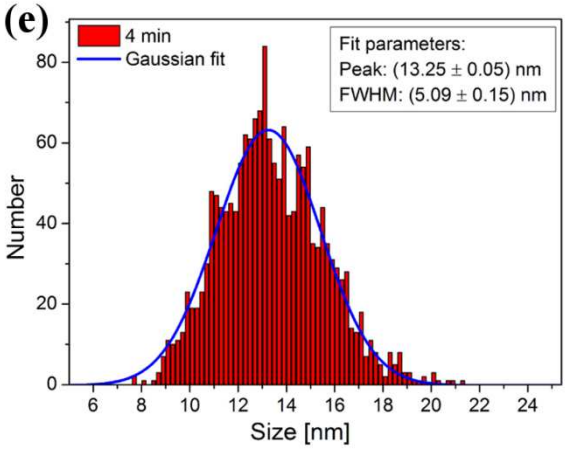

(f)

Nonlinear Curve Fit (Gauss) (23/05/2013 09:55:17)

Parameters

		Value	Standard Error
Number	y0	-0.13995	0.71686
	xc	13.25475	0.05279
	w	4.32586	0.12616
	A	343.47813	10.9805
	sigma	2.16293	0.06308
	FWHM	5.09331	0.14854
	Height	63.35295	1.43206

Reduced Chi-sqr = 22.9103288593
COD(R^2) = 0.9553347844024
Iterations Performed = 6
Total Iterations in Session = 7
Fit converged. Chi-Sqr tolerance value of 1E-9 was reached.
sigma, FWHM, Height are derived parameter(s).

Statistics

	Number
Number of Points	102
Degrees of Freedom	98
Reduced Chi-Sqr	22.91033
Residual Sum of Squares	2245.21223
Adj. R-Square	0.95397
Fit Status	Succeeded(100)

Fit Status Code :
100 : Fit converged. Chi-Sqr tolerance value of 1E-9 was reached

Figure S3-4: More TEMs for samples synthesized at 4 min microplasma exposure (a-d) scale bars: 50 nm, (e) particle size distribution with a fitted gaussian, (f) Origin fit report – parameters as in S3.1. (e&f) based on 1703 measurements sorted into 0.2 nm bins from 5 nm to 25.4 nm) From the raw data, min. size = 7.68 nm; max. size = 21.2 nm.

Comments regarding possible interpretation of TEMs: We have included a range of TEMs to provide visual information for the nanoparticles produced. We emphasize that these TEMs are complementary information to the UV-Vis, XRD, and EDX data provided which give information based on a much larger number of particles than is possible from a standard TEM image. The contrast in the TEMs may be interpreted in a number of ways, from faceting on the surface of the NP, to different crystalline features (recall in the main text we observed a range of crystalline planes from the XRD data from (311), (111), (200) and (220)), to different absorption of the electron beam by Au and Ag atoms. Due to the limitations of the TEM study in this particular work we cannot categorically ascribe the contrast to any one of these particular possibilities. Instead, we handled the data holistically and based our conclusions on all of the information (UV-Vis, XRD, EDX, TEM, HR-TEM) available to us.

Regarding Storage: Storage is indeed an issue that is important for nanoparticle synthesis. Our particles have good stability in water solution and can also be stored in a powder form after depositing on specially prepared surfaces. Although some particles appear agglomerated in TEM images, the extent of the agglomeration reduces at a longer process duration. To prevent the particles form agglomeration, whilst a surfactant was not used, a stabilizer (fructose) was indeed incorporated into the synthesis process (see ESI, Section S1).

S4: X-ray diffraction spectra

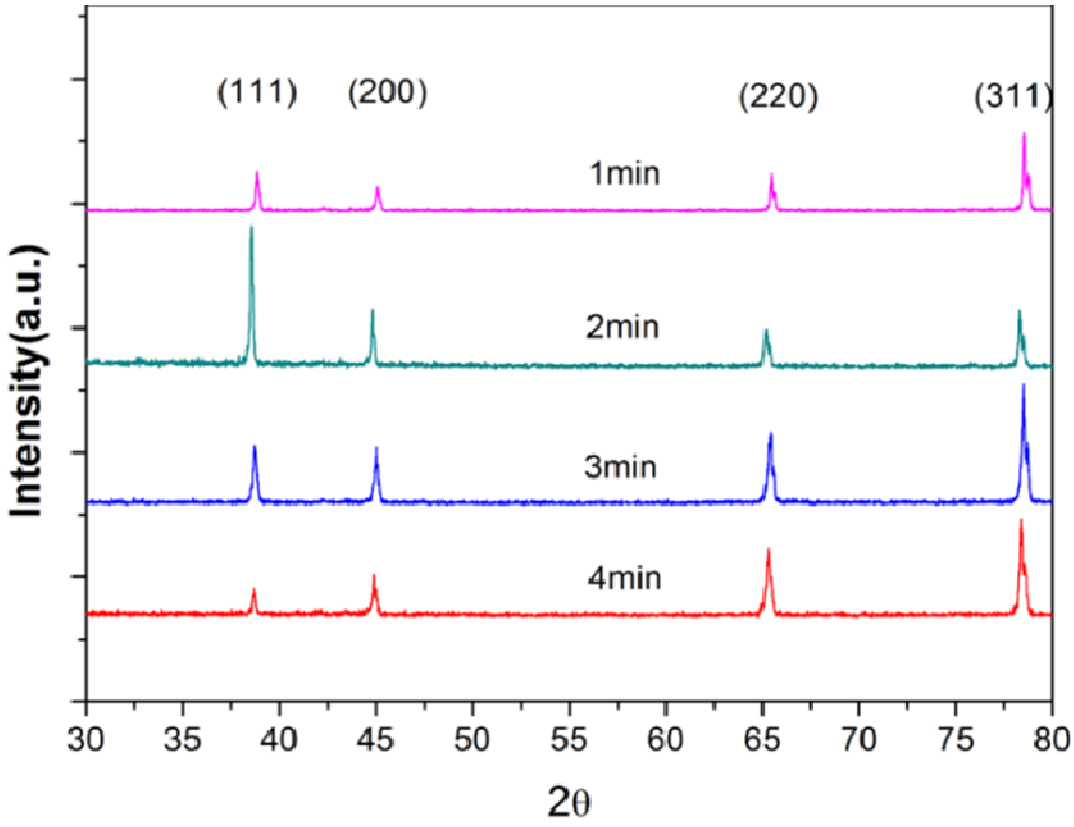

Figure S4-1: XRD spectra of the AuAg samples

X-ray diffraction spectra were acquired on Au_xAg_{1-x} samples in a powder form using a Scintag XDS-2000 diffractometer operated at 40 kV and 40 mA with CuK_α radiation and a diffracted beam monochromator (Bruker-D8 Advance), with 2θ ranging between 30 and 80^o.

The crystallinity of the NPs is evident from the X-ray diffraction data above in Figure S4-1 which shows clear peaks corresponding to the (111), (200), (220) and (311) crystal planes. We note that these XRD spectra demonstrate that crystalline alloys were obtained prior to exposure to an electron beam during HR-TEM analysis.

S5. Peak fit for UV-Vis absorbance data

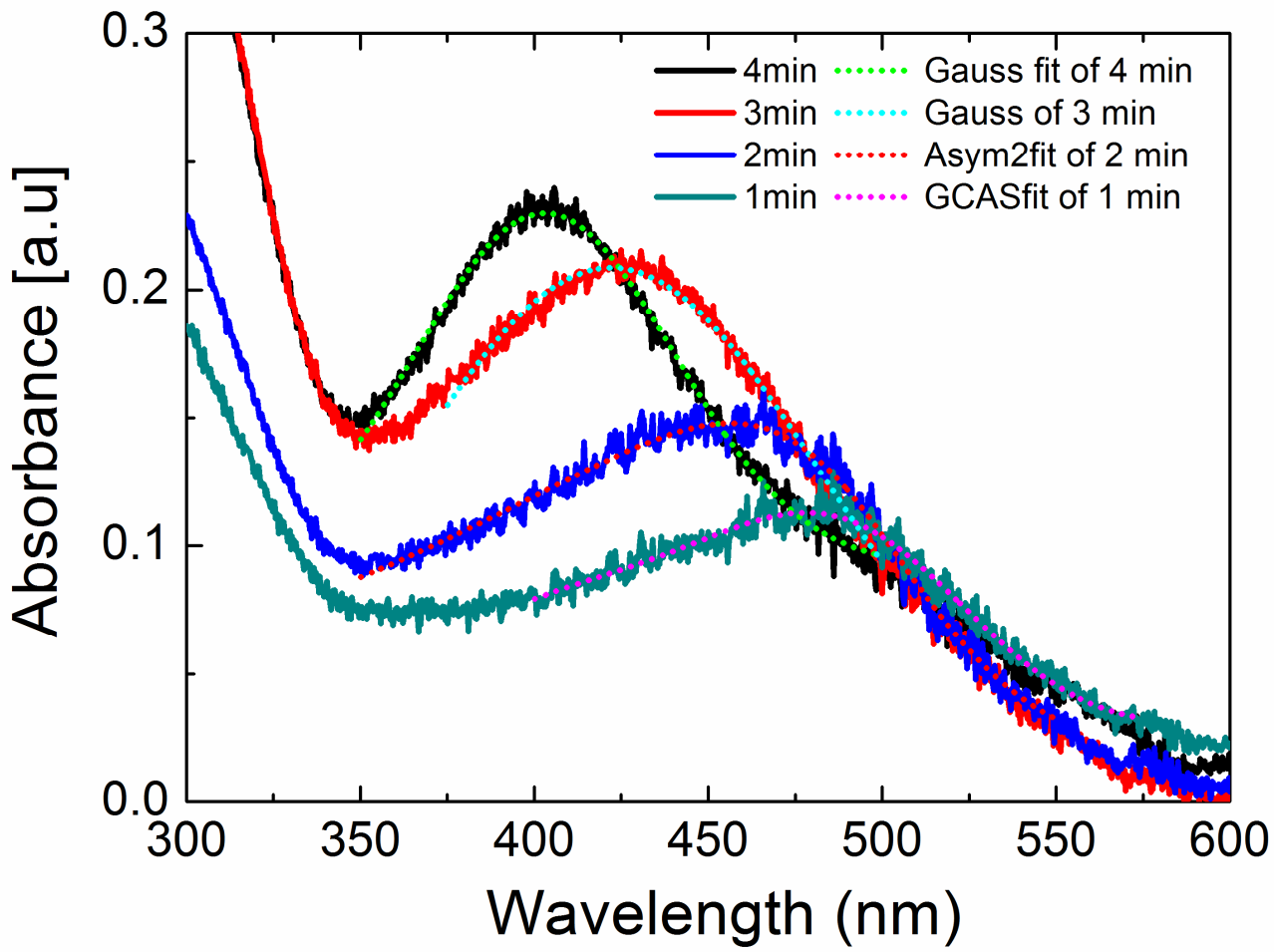

For 4 min and 3 min:

Description Nonlinear Curve Fit / Model Gauss

Equation y=y0 + (A/(w*sqrt(PI/2)))*exp(-2*((x-xc)/w)^2)

Parameter	*4min*	*4min (err)*	*3min*	*3min (err)*
y0	0.09155	6.86155E-4	0.00631	0.00862
xc	403.01576	0.10729	422.15392	0.16727
w	74.17857	0.46306	120.09764	3.48139
A	12.85313	0.12718	30.44452	2.14654
sigma	37.08928	0.23153	60.04882	1.7407
FWHM	87.33859	0.54521	141.40416	4.09902
Height	0.13825	6.61991E-4	0.20226	0.00845
Number of Points	533		446	
Degrees of Freedom	529		442	
Reduced Chi-Sqr	1.48689E-5		1.75697E-5	
Residual Sum of Squares	0.00787		0.00777	
Adj. R-Square	0.99265		0.98412	
Fit Status	Succeeded(100)		Succeeded(100)	

For 2 min and 1 min: From a quick peak find, based on fit data (asym2 and gcas fits for 2 and 1 min, respectively), the peaks for 1 min is approximately 486 nm and 2 min is approximately 463 nm

Time [min]	*PEAK LCN*	*ERR*
4	403.02	0.11
3	422.15	0.17
2	463.27	
1	486.15	

Peak wavelength has a clear pretty linear relationship with time (R^2 = 0.97)

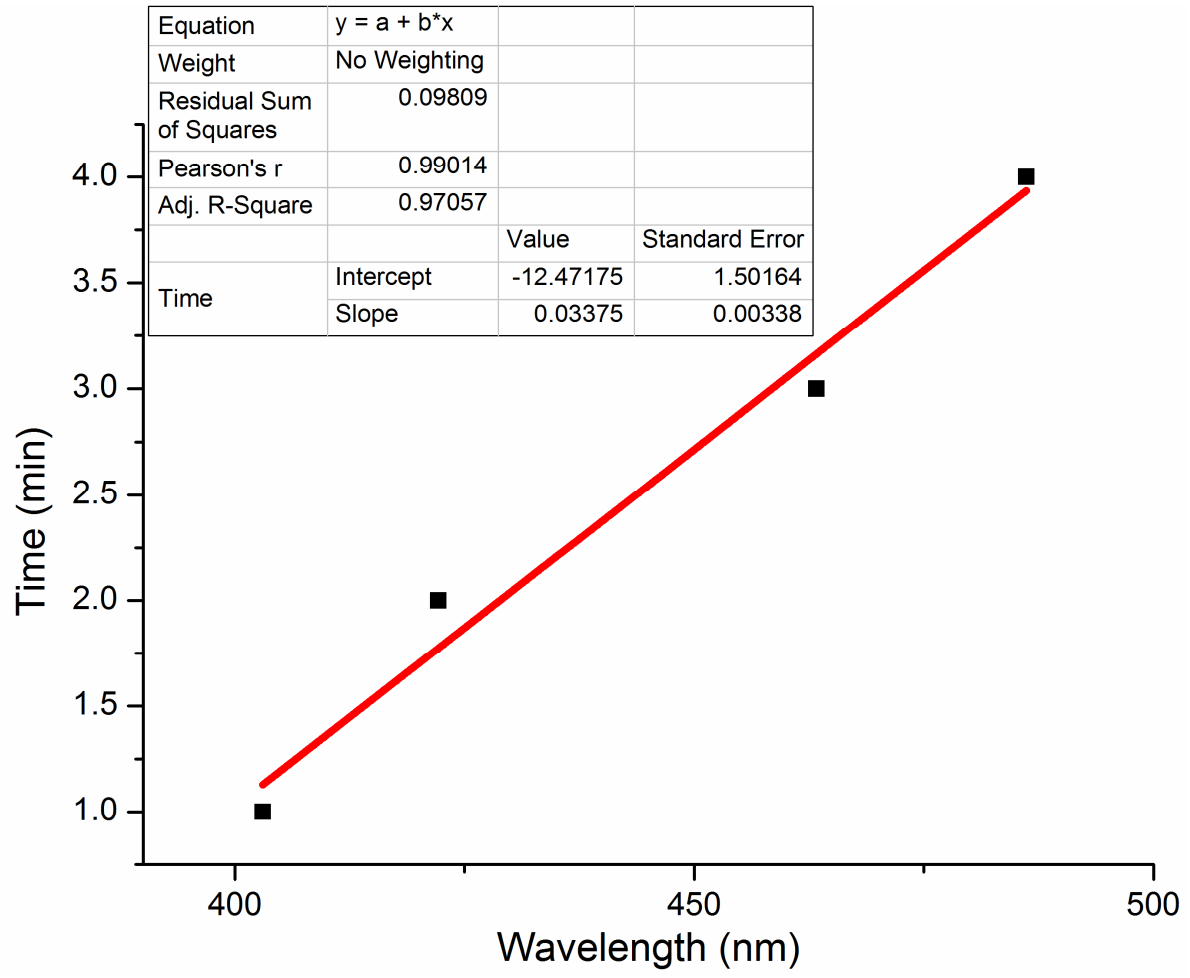

N.B. Peak fit data from inbuilt functions in Microcal Origin 8.6

S6: Evidence of suitability of technique to produce other alloys: AuPt

The microplasma-assisted electrochemical synthesis technique has been demonstrated for production of AuPt NPs, with the processing method as described in the main text (5 min processing time), but with different solutions as follows: $HPtCl_6$: 0.26 mM, $HAuCl_4$: 0.016 mM, Fructose: 8.4 mM. Below, sample TEMs, EDX and UV-Vis absorption spectra have been provided. More detailed results and analysis will appear in a future paper.

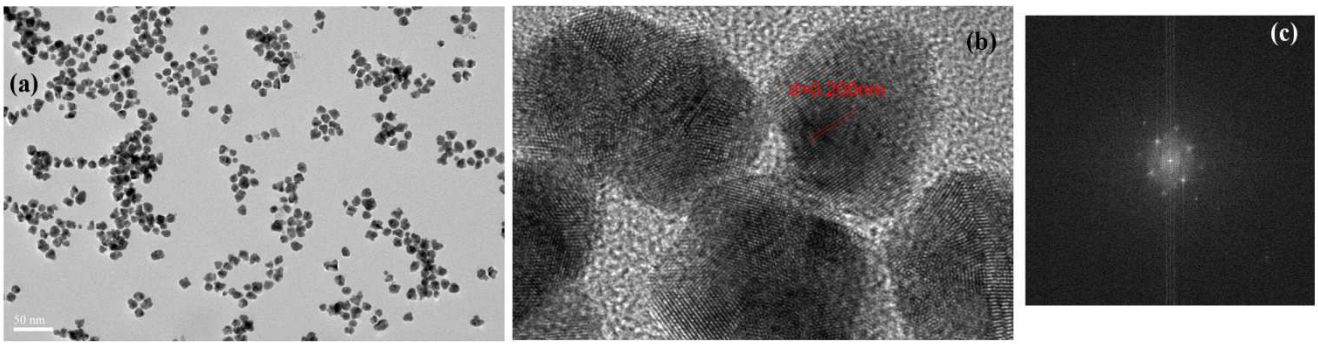

Figure S6-1: AuPt NP alloys (a) TEM, scale bar is 50 nm, (b) HR-TEM, with lattice spacing marked, (c) FFT of HR-TEM in (b).

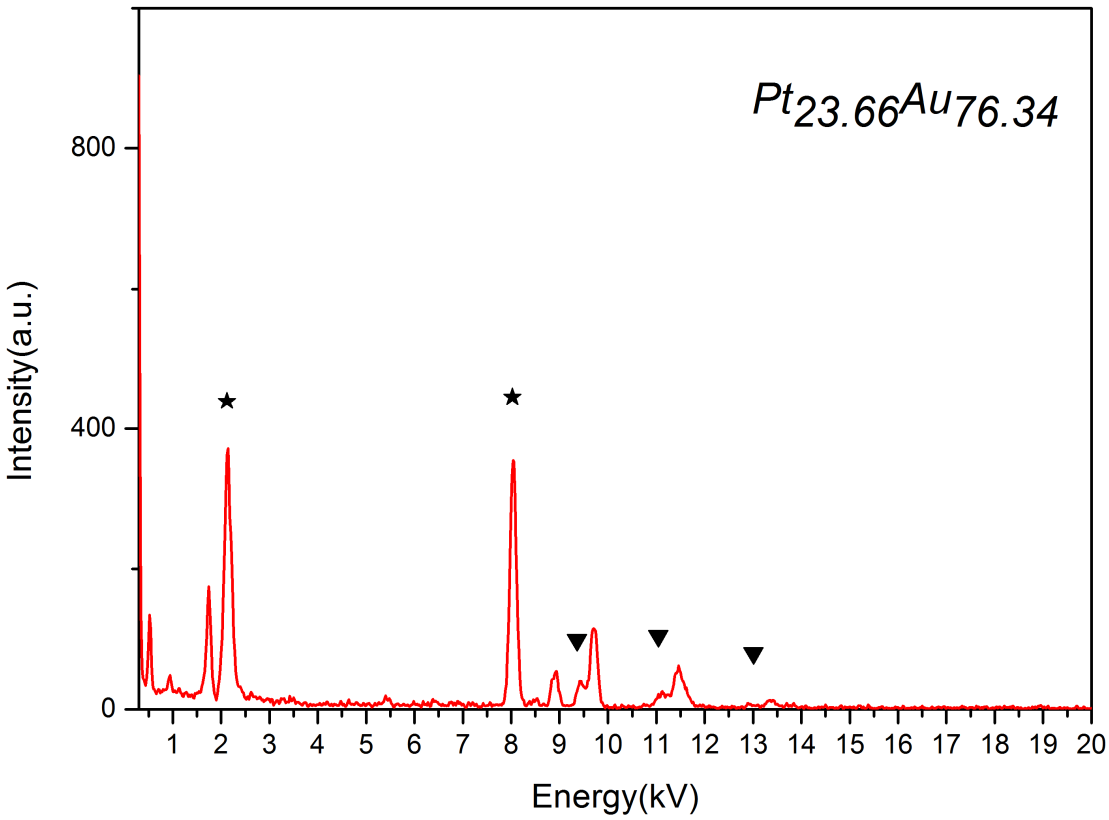

Figure S6-2: Energy Dispersive X-ray Spectroscopy of AuPt alloy NPs.

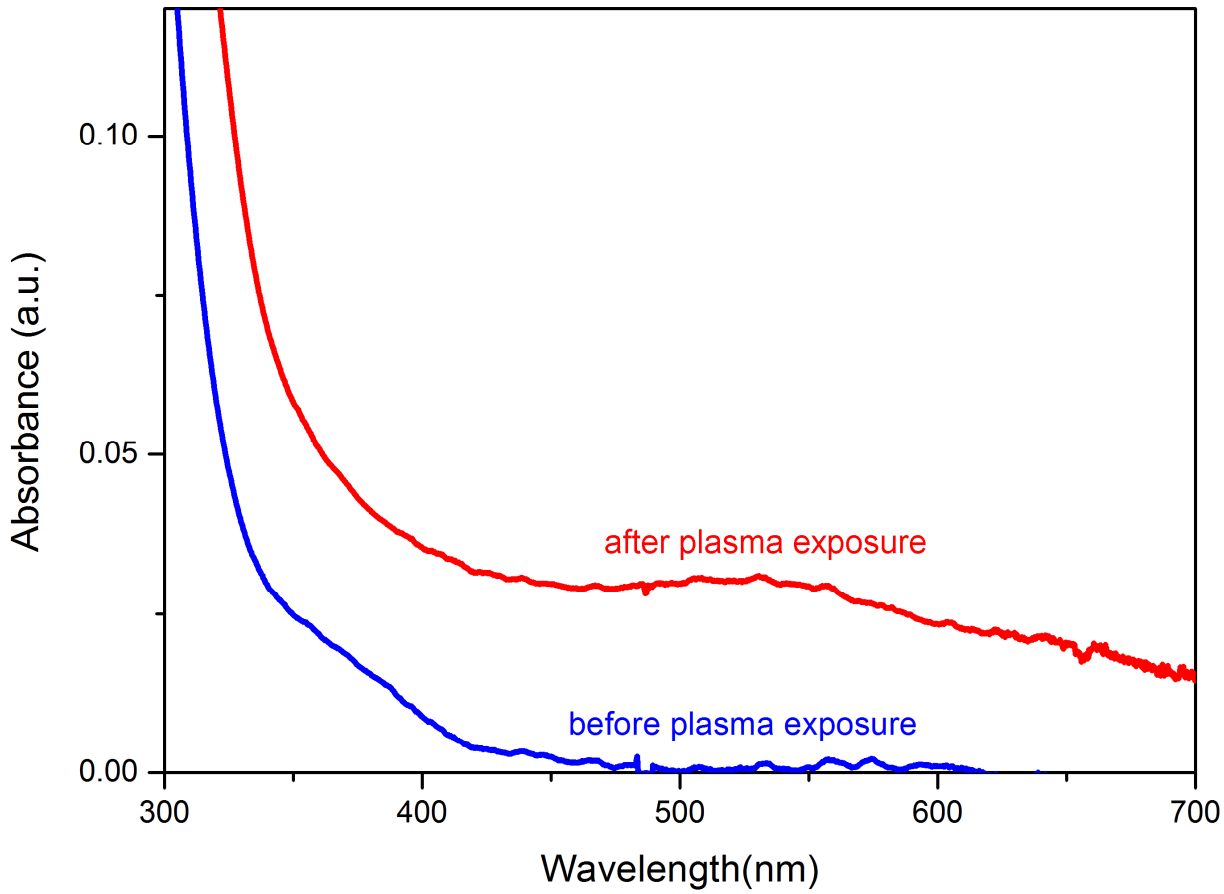

Figure S6-3: UV-Vis absorption spectra of samples before plasma exposure (blue line) and after plasma treatment for 5 min (red line).

S7: A discussion of typical microplasma-species and plasma-related effects on nanoparticle formation and a proposed mechanism for Au_xAg_{1-x} nanoparticle formation in liquid via microplasma-assisted electrochemistry.

(I) Typical He microplasma-species

Whilst diagnostic information regarding the exact species present in our He microplasma is not available, we can discuss the species that are likely present by referring to the available literature on atmospheric-pressure He microplasma jets, including the work of McKay et al.[R3] Note there may be some difference in species due to the capillary width (our jet has an inner cappilary width of 175 μm, whereas McKay *et al* consider widths of 530 μm), hence this section is included for illustration of the main points only.

McKay *et al* found their jet contained the following species:

- He^+, N^+, O^+, H_2O^+, N_2^+ and O_2^+ , $H^+(H_2O)_n$, where n = 3–55
- $O_3^-(H_2O)_n$, $CO_3^-(H_2O)_n$, $O_2^-(H_2O)_m$, $HCO_3^-(H_2O)_n$, $HO_2^-(H_2O)_n$ where n = 1–51 and m = 2–53.

In addition, readers interested in the diagnostics of microplasmas may find the following general review on the topic of interest:

Bruggeman, P., & Brandenburg, R. (2013). Atmospheric pressure discharge filaments and microplasmas: physics, chemistry and diagnostics. *Journal of Physics D: Applied Physics*, *46*(46), 464001. doi:10.1088/0022-3727/46/46/464001

(II) Plasma-related effects on nanoparticle formation

Our results represent a new viable approach based on reactive, highly non-equilibrium plasma chemistry.[R4-R10] Here, the plasma is indeed directly responsible for the alloyed AuAg synthesis. The most obvious evidence is that a similar process conducted in the same mixture of reagents and under the same temperature but without any plasma, does not produce these nanoparticles.

We believe that both metals are being reduced due to the microplasma, for 2 reasons:

Firstly, microplasmas have previously been shown to reduce both Au and Ag separately for nanoparticle synthesis [APL 93 (2008) 131501]. Thus, the plasma is capable of reducing both elements.

Secondly, based on our colour change observations in Figure 1 (c) – i.e., red first, indicating the NPs are more Au in nature, followed by the solution becoming increasingly green as time progresses indicating the NPs possess more silver. This is also reinforced by our UV-Vis spectra which show a blue shift with increasing time.

Aside from the above, there are 2 reasons why it may be that Au reduces first and solution becomes increasingly green (Ag) as time passes:

Reason 1: Au has a higher reduction potential – it is likely to be reduced quicker in solution than Ag.

Reason 2: There is less Au than Ag in the solution (ratio of 1:4), so it is used up very quickly, after which, the Ag is then reduced by the plasma.

Therefore, by the appropriate choice of the small ratio of Au (with respect to Ag) in the solution, the reduction of the two different elements takes place with a quite small time delay. For more details please see (III) below.

(III) Proposed mechanism for Au_xAg_{1-x} nanoparticle formation in liquid via microplasma-assisted electrochemistry

As discussed in the main text, silver and gold salts in solution undergo dissociation, forming ions which then undergo reduction, gaining electrons from the microplasma according to the following half cell reactions:

$Au^{3+}(aq) + 3e^- \rightarrow Au(s)$; $E^o = 1.52$ V [R1]

$Ag^+(aq) + e^- \rightarrow Ag(s)$; $E^o = 0.799$ V [R1]

The Au and Ag may then agglomerate and form nanoparticles. However, these energetic electrons from the microplasma may also interact with the H_2O in the mixture as follows:

$e^- + H_2O \rightarrow H^* + OH^-$

$e^- + H^+ \rightarrow H^*$

$H^* + M^+ \rightarrow H^+ + M^*$

Please note,

- H^* is a hydrogen atom, which is unstable, so we label it as a radical.
- M^* is a metal atom, which is stable, so we just call it M.
- Then: $nH^* + M^{n+} \rightarrow nH^+ + M$

The M (i.e. where M is a neutral metal atom, in this case, Ag or Au) may then go on to form new NP nuclei or add onto existing NP nuclei (where 'N' is the number of atoms), i.e.

$NP^N + M \rightarrow NP^{N+1}$

The other possibility is that these H radicals act as catalysts and cause rearrangement of the NP surface into a more crystalline configuration than typically observed in citrate-produced alloyed NPs .

Another group,[R2] when studying the nucleation of Au NPs in H_2O via plasma only-chemistry (no other materials in solution, just $HAuCl_4$ and H_2O, Au NP nucleation assumed to only

happen due to the presence of the plasma) have proposed that reduction of $HAuCl_4$ may be via hydrogen peroxide and proceed via the following mechanism.[R2]

$$e^-_{plasma} + H_2O \rightarrow OH^* + H^-$$
$$2OH^* \rightarrow H_2O_2$$
$$3H_2O_2 + 3OH^- + Au^{3+} \rightarrow Au^0 + 3HO_2 + 3H_2O$$

As we have a number of different species in solution ($HAuCl_4$,$AgNO_3$, H_2O, Fructose) it is unlikely that this would be the sole mechanism occurring in our Au_xAg_{1-x} NP synthesis. However, it may be one of the many reactions that would take place in the mixture, in addition to the reactions posited above.

That being said, we note that reaction kinetics is not the main point of this work. As basic reaction kinetics are well known, we refer the reader to relevant literature/text books (i.e. Silverberg, M. S. *Chemistry: The Molecular Nature of Matter and Change*; 3rd Edition.; McGraw-Hill: New York, NY, 2003) and dedicated in-depth studies concerning plasma-liquid interactions can be found elsewhere.[R10]

S8: Comparison of microplasma-assisted electrochemistry to UV-, microwave-, and ultrasound-based synthesis methods and comments regarding potential applications:

Whilst plasma is an excited state of matter, we note that the plasma-assisted method is a conceptually different approach compared to the microwave, UV- and ultrasound assisted techniques; this approach is also very different in the execution in a number of ways.

- Firstly, the plasma contains a number of agents not used in the aforementioned techniques, namely electrons, ions and radicals. These species are active in the reduction and nucleation process for AuAg alloyed nanoparticles.
- Secondly, the equipment involved in the plasma-case is much easier to use, for example compared to very expensive microwave equipment with serious health-related issues.
- Thirdly, these methods do not produce fine, crystalline, well alloyed AuAg NPs as we have demonstrated in our work

Comments regarding potential applications: Whilst we note that the main point of our work is proof of principle, not a demonstration of the superiority of the AuAg in a specific application. The size-dependent plasmonic response of the AuAg nanoparticles is a clear indication of potential applications, for example for labeling the flow in the flow chemistry systems that are rapidly gaining momentum.

S9: References to Supporting Information

R1 Tables of Physical & Chemical Constants (16th edition 1995). 3.9.3 Standard potentials at 25 ^{o}C. Kaye & Laby Online. Version 1.0 (2005) www.kayelaby.npl.co.uk

R2 Patel *et al*., *Nanotechnology* 2013, **24**, 245604

R3 K. McKay, J.-S. Oh, J. L. Walsh, and J. W. Bradley, *J. Phys. D. Appl. Phys.*, 2013, **46**, 464018.

R4 J. Zheng, R. Yang, L. Xie, J. Qu, Y. Liu, X. Li, *Adv. Mater*. 2010, **22**, 1451.

R5 E. C. Neyts, A. C. T. van Duin, A. Bogaerts, *J. Am. Chem. Soc.* 2012, **134**, 1256.

R6 M. Meyyappan, *J. Phys. D.: Appl. Phys.* 2009, **42**, 213001.

R7 U. Cvelbar, Z. Chen, M. K. Sunkara, M. Mozetič, *Small* 2008, **4**, 1610.

R8 M. G. Kong, M. Keidar, K. Ostrikov, *J. Phys. D: Appl. Phys*. 2011, **44**, 174018.

R9 D. Mariotti, R. M. Sankaran, *J. Phys. D: Appl. Phys.* 2010, **43**, 323001.

R10 D. Mariotti, J. Patel, V. Svrcek, P. Maguire, *Plasma Proc. Polym.* 2012, **9**, 1074